Advances in Geo-Energy Research

Vol. 21, No. 3, p. 238-246, 2026

Original article

Discrepancies between macroscopic kinetics and microscopic cage-filling behavior of CH_4 hydrate growth in fine-grained sediments: A multi-scale analysis

Xuebing Zhou[1,2], Gelin Chen[1,2], Chenlu Xu[3]*, Yong Chen[1], Ye Zhang[4], Deqing Liang[1,2]*

[1]*Guangzhou Institute of Energy Conversion, Chinese Academy of Sciences, Guangzhou 510640, P. R. China*

[2]*School of Energy Science and Engineering, University of Science and Technology of China, Hefei 230026, P. R. China*

[3]*Guangzhou Marine Geological Survey, China Geological Survey, Guangzhou 510075, P. R. China*

[4]*Department of Chemical and Biomolecular Engineering, National University of Singapore, Singapore 117582, Singapore*

Keywords:
CH_4 hydrate
porous media
in-situ Raman spectroscopy
hydrate growth

Cited as:
Zhou, X., Chen, G., Xu, C., Chen, Y., Zhang, Y., Liang, D. Discrepancies between macroscopic kinetics and microscopic cage-filling behavior of CH_4 hydrate growth in fine-grained sediments: A multi-scale analysis. Advances in Geo-Energy Research, 2026, 21(3): 238-246.
https://doi.org/10.46690/ager.2026.09.04

Abstract:
To clarify the growth of CH_4 hydrate in fine-grained sediments, samples with specific water saturation were tested using macroscopic experiments and *in-situ* Raman spectroscopy under specific temperature and pressure conditions. The Raman spectra were quantitatively analyzed to track hydration numbers and CH_4 occupancy in large and small cages. The results showed that the newly formed hydrate nuclei were highly unsaturated, and large cage occupancy rose rapidly to a plateau, while small cage filling remained negligible throughout the growth process. Both the macroscopic and the spectroscopy data showed that the fractional pore water remained unconverted, which was attributed to capillary pressure elevation by the pore hydrates. Notably, the macroscopic initial gas consumption rate decreased with increasing temperature, which was opposite to the faster cage filling at higher temperatures as observed by *in-situ* Raman spectroscopy. This latter trend supports a two-stage mechanism, where lower temperatures promote the rapid spreading of unsaturated nuclei, thus providing abundant adsorption sites, whereas higher temperatures enhance intrinsic gas adsorption but suppressed nuclei spreading, thereby reducing the gas consumption rate in macroscopic measurements. These findings challenge the common assumption of fully occupied cages in nascent hydrates and emphasize the necessity of distinguishing between nucleation-controlled and mass-transfer-controlled stages in hydrate growth kinetics.

1. Introduction

Naturally occurring gas hydrates are solid crystalline materials formed by hydrocarbon gases and water under low temperature and high pressure, conditions commonly found in ocean sediments on continental margins and permafrost. The in-situ gas volume of hydrates is approximately 3×10^{15} m^3 on a global scale, exceeding 1.56 times the conventional natural gas reserves (Shaibu et al., 2021; Pang et al., 2025). Beyond natural occurrence, hydrate-based technologies, including solidified natural gas storage, gas separation, carbon sequestration, and seawater desalination, have drawn increasing attention in chemical engineering (Zheng et al., 2019; Chen et al., 2025; Liu et al., 2025). Among all the hydrate synthesis and storage systems being researched, those in porous media are the most common and complex. In such media, hydrate formation is a coupled process involving phase change, heat transfer and multicomponent mass transport, all strongly mo-

Yandy Scientific Press

*Corresponding author.
E-mail address: zhouxb@ms.giec.ac.cn (X. Zhou); chengelin@mail.ustc.edu.cn (G. Chen); gmgsxcl@126.com (C. Xu); chenyong1@ms.giec.ac.cn (Y. Chen); zhang.ye@nus.edu.sg (Y. Zhang); liangdq@ms.giec.ac.cn (D. Liang).
2207-9963 © The Author(s) 2026.
Received July 20, 2026; revised August 9, 2026; accepted August 19, 2026; available online August 21, 2026.

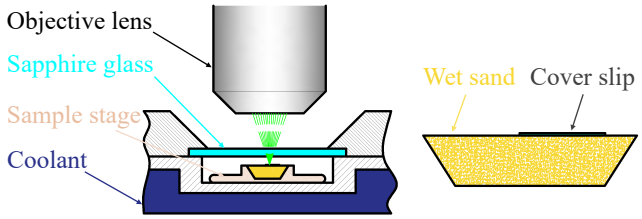


Fig. 1. Configuration of the *in-situ* Raman device.

dulated by sediment properties and environmental conditions (Qin et al., 2022; Li et al., 2026). Therefore, a quantitative understanding of hydrate growth is essential for both resource assessment and process intensification (Hu et al., 2024).

The hydrate formation process in porous media is generally influenced by 3 main factors: Sediments, gas-liquid fluids, and the hydrates themselves. Sediments alter the hydrate growth process primarily through bound water, capillary pressure and thermal conductivity (Zhu et al., 2023). Sun et al. (2021) found that bound water in porous media, including interlayer bound water in clay and adsorbed water on particle surfaces, is more difficult to convert into hydrate. In the presence of montmorillonite, the conversion rate of bound water hydrates in clay is only about one-third of that in sandy pore water (Feng et al., 2023; Xie et al., 2024). Uchida et al. (2002) noted that capillary force is the one of the major reasons for the leftward shift of the hydrate equilibrium curve under small pore size conditions. When the particle size is below 0.1 mm, a significant shift in the phase equilibrium conditions will occur (Zhou et al., 2024, 2025).

Gas and liquid properties constrain hydrate growth via gas component and water activity and surface tension. By measuring the thermal stabilities of the hydrates formed from methane, ethane and propane in porous media, Lee et al. (2010) and Avaji et al. (2023) found that the influence of propane is more evident than that of ethane, with a maximum offset of about 12 K. Mu and Cui (2019) found that the effect of CO_2 on the rightward shift of the phase equilibrium curve is relatively weak, and even with a CO_2 content up to 79.8 mol%, its offset was much smaller than that of the system containing a small amount of propane. Water activity and surface tension are mainly affected by additives in the aqueous phase, including surfactants and organic and inorganic salts in the liquid phase (Tegze et al., 2006; Kumar et al., 2015; Ke et al., 2019). To control hydrate formation, a series of hydrate promoters and inhibitors have been developed. Although their mechanisms of action are different at the microscale, they generally take effect by changing the concentration and stability of water molecule clusters or controlling gas transport in the aqueous phase (Das et al., 2022; Liu et al., 2024; Zhao et al., 2025a).

In contrast to the two factors mentioned above, the influence of hydrates has been frequently noted but barely investigated. In most studies, pore hydrates are assumed as stable solids with a constant hydration number, so that the parameters such as hydrate growth rate and residual water in porous media could be quantitatively determined (Fukumoto et al., 2018; Moridis et al., 2019; Rehman et al., 2025). However, such an assumption has proved to be unsuitable at the microscopic level. First, formed pore hydrates have stronger wettability than sediment, which can create more bond water and higher capillary pressure (Nikitin et al., 2020; Wu, 2023; Li et al., 2024). This may in turn lead to a more evident inhibitory effect on hydrate equilibrium due to the high hydrate saturation. Second, gas saturation in the hydrate phase is rarely constant but evolves dynamically during formation. Zhou et al. (2021) observed that hydrate growth initiates from highly unsaturated nuclei and approaches apparent stability through continuous gas adsorption, implying a kinetically driven non-stoichiometric pathway. Yang et al. (2023) further quantified the hydration number in clay minerals using nuclear magnetic resonance, reporting values above 6.5, which significantly exceed the ideal stoichiometric ratio for sI hydrate. Together, these findings indicate that cage occupancy is influenced by growth stage and pore confinement, thereby challenging the conventional assumption of a fixed hydration number in porous media. When coupled with the heat and mass transfer resistances induced by hydrate growth, such non-ideal characteristics underscore that hydrate itself constitutes a critical factor that cannot be overlooked in hydrate formation studies. In this work, to reveal the influence of pore hydrate on hydrate formation in porous media, hydrate growth in fine-grained sediments was measured at multiple scales. Macroscopically, CH_4 hydrate was allowed to grow in hollow and solid fine-grained columns at different temperature, and the gas consumptions were calculated to reveal the hydrate growth rate. Meanwhile, *in-situ* Raman spectroscopy was employed to measure the gas distribution during hydrate formation. By correlating gas migration behaviors at multiple scales, the effect of hydrate saturation on hydrate formation could be revealed.

2. Materials and methods

2.1 Apparatus and materials

The experimental apparatus used in this experiment was a cylindrical high-pressure reactor with an effective volume of 159 ± 0.8 mL and an internal diameter of 70 mm. A pressure transmitter and a platinum resistance thermometer were set on the cap of the reactor, with accuracies of ± 0.001 MPa and ± 0.1 K, respectively. The temperature was controlled by immersing the reactor in a water bath, that had a temperature fluctuation of ± 0.1 K. Temperature and pressure were recorded by data acquisition at 10 s intervals.

The *in-situ* Raman spectroscopy measurements were performed using a custom-designed cell capable of withstanding up to 12 MPa, as seen in Fig. 1. A 6 mm-thick sapphire glass was covered on the sample chamber to allow direct contact with the vertical incidence of the laser beam. The sample temperature was controlled by a water bath with an accuracy of ± 0.1 K, while two additional high-pressure vessels connected to the inlet and outlet stabilized the pressure within ± 0.01 MPa. A confocal Raman spectrometer (Horiba, LabRAM HR) equipped with a multichannel air-cooled detector and an Ar^+ laser (532 nm, maximum power 50 mW) was used for spectral acquisition. The instrument was calibrated against a silicon crystal standard (Raman shift 520.7 cm^{-1} at 300 K).

The materials used for CH_4 hydrate formation included

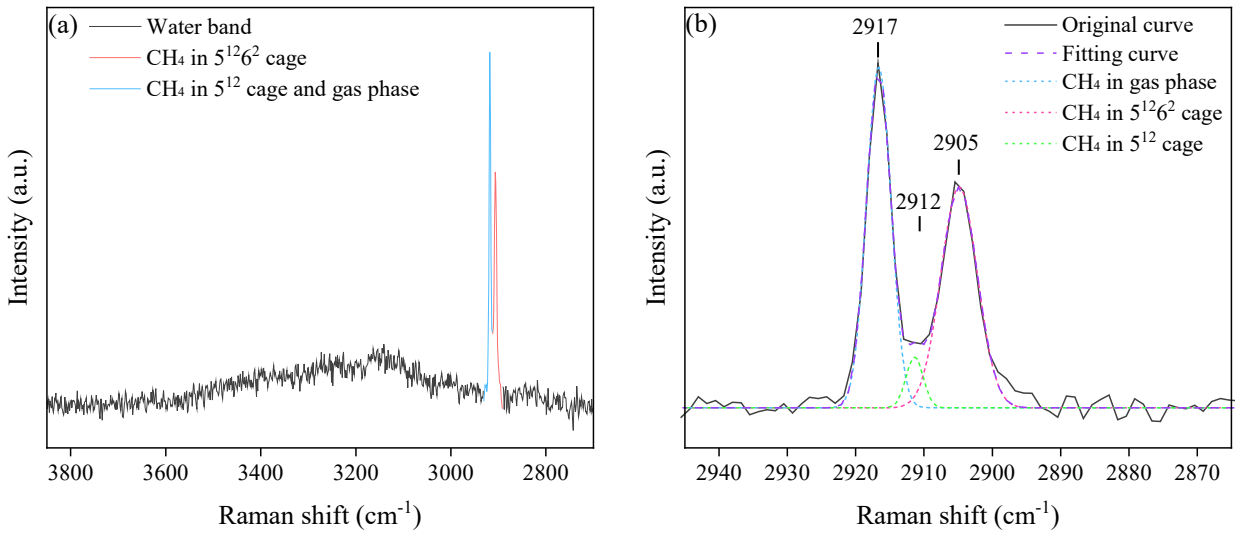


Fig. 2. Characteristic peaks of Raman spectra: (a) large cage (2,905 cm^{-1}) and gas phase (2,917 cm^{-1}) peaks and (b) small cage (2,912 cm^{-1}) peak.

methane, deionized water, and fine-grained sediment. The pressurized methane used had 99.9 mol% purity. Fine-grained sediment was collected from the Pearl River, China, carefully washed, and sieved to a particle size range from 0.025 to 0.055 mm. The porosity and density of the fine-grained sediment were 41.48% and 1.60 g/cm^3, respectively. Deionized water was prepared in the laboratory, that featured 18.2 MΩ·cm resistivity.

2.2 *In-situ* Raman spectroscopy

The *in-situ* Raman measurements were taken under the same conditions as the macroscopic measurements. Fine-grained sediment samples with certain water content were tightly compacted into the sample loader and sealed in the high-pressure chamber of the Raman reactor. To simulate the growth of pore hydrates, a cover slip was placed above the wet sediment, as seen in Fig. 1. After the chamber temperature was lowered to the set value, it was flushed with CH_4, and rapidly then pressurized to the target value. During the initial stage of hydrate growth, spectra were recorded every 5 min. Once the intensity of the characteristic peak of CH_4 no longer increased rapidly, the scanning frequency was gradually reduced until the peak intensity stabilized. The acquired Raman spectra were used to analyze the CH_4 occupancy in hydrate cages and the evolution of gas concentration during hydrate growth. The normalization method, which uses the area ratio of the CH_4 peak to the water bending band, has been validated in our previous work (Zhou et al., 2025). The reproducibility of the peak area ratios was within ±5% based on repeated measurements under the same conditions. The main sources of error include spectral baseline fluctuations, laser intensity drift, and variations in the focal plane, which were minimized by averaging 10 accumulations per spectrum and by daily calibration against a silicon standard.

2.3 Macroscopic measurements

To prepare the sediment samples, the sediment was pre-mixed with a certain amount of water. To ensure uniform porosity, the wet sediment was densely packed so that the water saturation was identical in hollow sediment columns. The hollow sediment column had the inner and outer diameters of 60 and 70 mm, respectively, which was tightly adhered to the wall of the reactor. After packing, the reactor was sealed, evacuated and immersed in a water bath pre-cooled at 276 K for 12 h to avoid any premature hydrate formation. Finally, the reactor was pressurized to 6 MPa and no additional CH_4 was added during hydrate formation. The temperature and pressure of the gas phase were recorded during hydrate formation. The CH_4 consumption for hydrate growth was calculated using the P-R equation of state (Vitu et al., 2008; Plee et al., 2015). The experiment was terminated when the pressure decay was less than 0.01 MPa within 2 h. Each experiment was repeated 3-5 times to ensure reproducibility.

3. Results and discussion

3.1 Growth of hydrate nuclei

To elucidate the growth behavior and rate-limiting step, *in-situ* Raman spectroscopy was used to measure the growth of CH_4 concentration in the hydrate phase. Fig. 2 shows the Raman spectra of CH_4 hydrate in fine-grained sediment under equilibrium state. Two peaks can be seen at 2,905 cm^{-1} and 2,917 cm^{-1} (Fig. 2(a)), which were assigned to be the CH_4 in the large cage ($5^{12}6^2$ cage) of sI hydrate and the gas phase in fine-grained sediment. Another peak that lay between these two peaks at about 2,912 cm^{-1} was the CH_4 in the small cage (5^{12} cage) of sI hydrate (Fig. 2(b)). The positions of those peaks were generally consistent with literature data (Zhou et al., 2021, 2025; Qiu et al., 2026).

The *in-situ* Raman spectra of CH_4 hydrate growth in fine-grained sediment are shown in Fig. 3. All measurements were

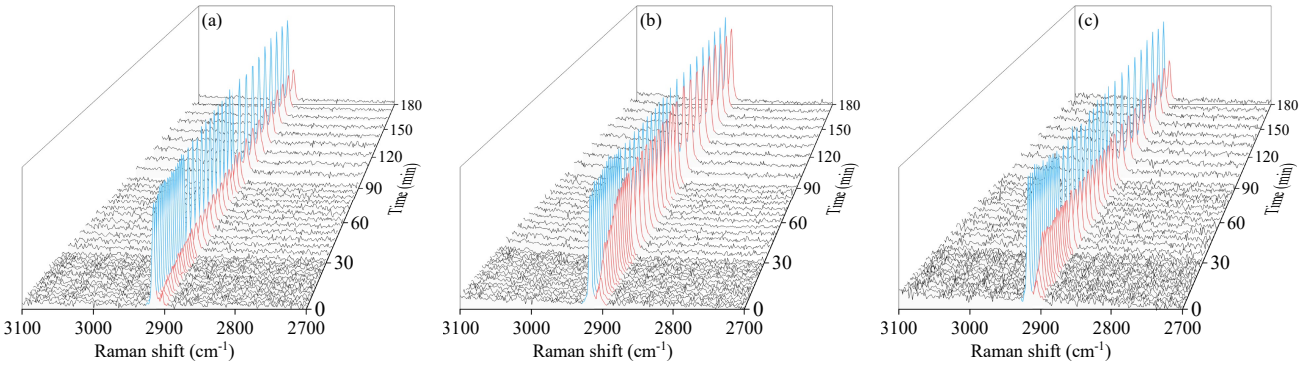


Fig. 3. *In-situ* Raman spectra of CH_4 hydrate growth in fine-gained sediment at (a) 274.15, (b) 276.15 and (c) 278.15K.

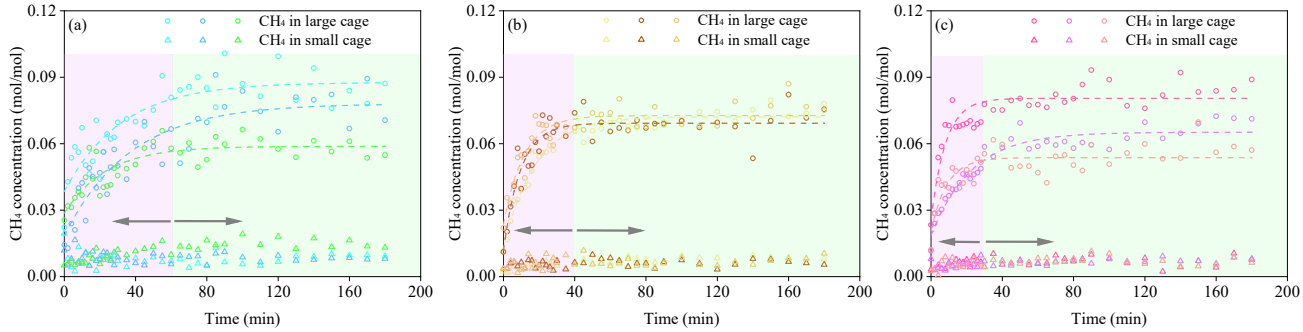


Fig. 4. Temporal evolution of CH_4 concentration in the large and small cages of sI hydrate at (a) 274.15, (b) 276.15 and (c) 278.15 K.

carried out under 6 MPa with an initial water saturation of 50%. In the 180-min test, the gaseous CH_4 peaks remained relatively steady, suggesting that the gaseous CH_4 do not have a significant change in hydrate growth. The major difference lies in the peak at 2,905 cm^{-1} representing CH_4 in the large cage of sI hydrate. This exhibits a rapid initial surge followed by a gradual approach to a saturation plateau, characteristic of an exponential rise to a maximum. Therefore, CH_4 hydrate growth in porous media is not a second-scale reaction but a minute-scale process. The limiting effect of fine-grained sediment particles on pore water and hydrate nucleus displacement may be the main factor restricting hydrate growth. In addition, the growth of 2,905 cm^{-1} peak was found to reach stability faster at high temperature, suggesting that higher temperature promotes the growth of hydrate nuclei.

To provide a clear insight into the CH_4 concentration change in the large and small cages of hydrates, the temporal evolution of Raman peak at 2,905 cm^{-1} and 2,912 cm^{-1} was extracted and normalized to correlate with CH_4 concentration. This correlation method is based on the fact that the normalized CH_4 peak area is proportional to the concentration of CH_4 in the hydrate and the liquid phase (Zhou et al., 2021). The normalization of CH_4 characteristic peaks was achieved by dividing the CH_4 peak area by the area of water band; with detailed information found in the literature (Zhou et al., 2025). To isolate the hydrate-phase signals, the Raman spectra were baseline-corrected and fitted with multiple Lorentzian functions. The contribution from dissolved CH_4 in the liquid phase, which was weak under the applied conditions, was estimated from spectra recorded prior to hydrate nucleation and subtracted as a background. This procedure ensured that the reported small-cage peak areas predominantly reflected CH_4 in the hydrate phase. It should be noted that the CH_4 concentration obtained by this calculation method refers to averaged concentrations in the liquid and hydrate phase, because the water peak intensities in the Raman spectra is jointly contributed by water molecules in the liquid and hydrate phases.

To elucidate the temporal evolution of cage-specific methane occupancy during hydrate nucleation and growth, the normalized peak areas of the large (2,905 cm^{-1}) and small (2,912 cm^{-1}) cages were extracted. As seen in Fig. 4, the large-cage concentration exhibits a rapid initial increase followed by a gradual approach to a plateau, whereas the small-cage signal remains nearly constant at a low level (~0.04) throughout the entire growth period. This observation indicates that methane occupation in the small cages is already saturated prior to hydrate nucleation, while the newly formed nuclei are primarily stabilized by large-cage filling. While the CH_4 concentration in the large cages exhibits a sharp rise, it is followed by a gradual approach to a saturation plateau in a range from 0.04 to 0.06. Therefore, it is reasonable to believe that the gas consumed for hydrate growth is mainly adsorbed by the large hydrate cages. In other words, the newly formed hydrate nuclei are highly unsaturated. Such a conclusion is generally in accord with our previous work performed on ice powder (Zhou et al., 2021); however, it is still inconsistent with the results of molecular simulations. Therein, the growth

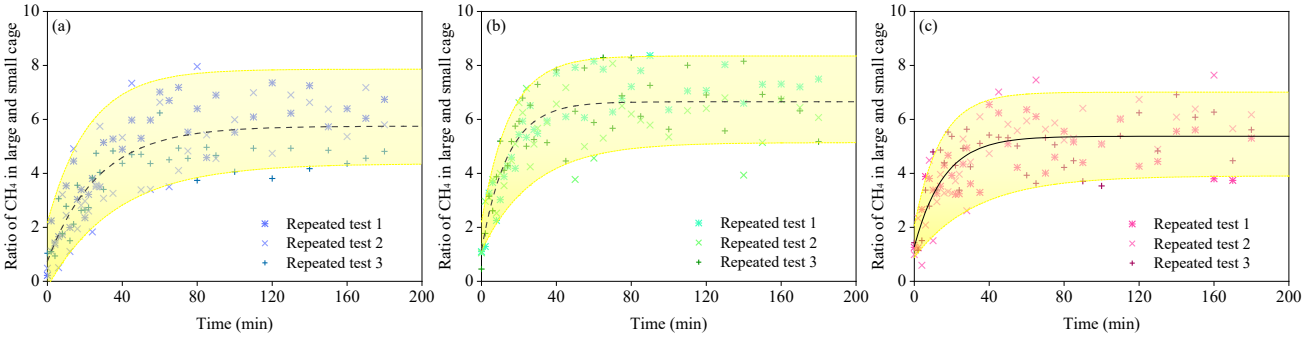


Fig. 5. Ratio of CH_4 in the large and small cages at (a) 274.15, (b) 276.15 and (c) 278.15 K.

Table 1. Hydration numbers, $R_{L\text{-}S}$ and $R_{L\text{-}H}$ obtained at saturation state.

Test	Temperature (K)	$R_{L\text{-}S}$	Hydration number	$R_{L\text{-}H}$
1	274.15	6.548 ± 0.257	6.651 ± 0.035	0.445 ± 0.039
2	274.15	6.286 ± 0.531	6.614 ± 0.077	0.591 ± 0.060
3	274.15	4.691 ± 0.167	6.320 ± 0.040	0.895 ± 0.053
4	276.15	5.949 ± 0.223	6.563 ± 0.035	0.718 ± 0.019
5	276.15	6.705 ± 0.222	6.672 ± 0.029	0.785 ± 0.028
6	276.15	6.655 ± 0.134	6.665 ± 0.018	0.707 ± 0.026
7	278.15	4.990 ± 0.206	6.387 ± 0.044	0.624 ± 0.025
8	278.15	6.199 ± 0.275	6.602 ± 0.041	0.861 ± 0.030
9	278.15	5.043 ± 0.184	6.398 ± 0.039	1.251 ± 0.046

of hydrate nuclei must rely on full occupancy of gas molecules in the cage structure, especially in large cages (Walsh et al., 2009; Zhang et al., 2015; Zhong et al., 2025). Consequently, the continuous growth of hydrate crystals must be based on the complete occupancy of the original hydrate cage structure by guest molecules (Liu et al., 2023).

The effect of temperature rise on the growth of hydrates is mainly shown as the promotive effect of gas adsorption of large hydrate cages, which is generally consistent with previous work (Sun et al., 2025). As the temperature was increased from 274.15 to 278.15K, the time consumed for hydrate growth reduced from about 60 mins to 40 and 25 mins, respectively, as seen in Fig. 5. Due to measurement errors, it is difficult to accurately measure the temperature effect on the concentration of hydrates at adsorption saturation. However, the saturated CH_4 concentration mainly fluctuated between 0.04 and 0.06, and did not show a significant upward trend with the temperature rise.

To further reveal the cage occupancy of CH_4 in pore hydrate, the ratio of CH_4 in large and small cages ($R_{L\text{-}S}$) were calculated. By assuming that the large hydrate cage is fully occupied at the saturated state, CH_4 occupancies in the small cages and the hydration number could be obtained. As seen in Fig. 5, the profiles of R_{L-S} are quite similar to the growth in CH_4 concentration in the large cages because the CH_4 concentrations in small cages remains almost unchanged during hydrate growth. The saturated ratios fluctuate in the range of 4.5 to 6.5, which were not found be greatly affected by temperature. In this case, CH_4 occupancies in small cages and the hydration number could be calculated as seen in Table 1. The hydration numbers range from 6.3 to 6.8, which is generally in line with the literature (Yang et al., 2023; Rossi et al., 2023). Only half of small cages are occupied by CH_4 molecules, suggesting that each hydrate unit cell contains only one CH_4 molecule in newly formed nuclei. Such a phenomenon indicates that the sI hydrate can possibly form without guest molecules, providing a formation pathway of a new structure of ice (Zheng et al., 2022; Zhao et al., 2025b). The observation of very low small-cage occupancy may appear contradictory to classical equilibrium thermodynamics, which requires full occupancy for stability. However, our experiments were performed under high supersaturation and rapid nucleation, where kinetic effects dominate. Non-equilibrium simulations and experimental studies have reported the existence of metastable clathrate structures with partial cage occupancy (Walsh et al., 2009; Zhao et al., 2025b; Zhong et al., 2025). In particular, Zhou et al. (2021) observed similar behavior during hydrate growth from ice, where small cages were filled only gradually after prolonged annealing. Therefore, the current results are interpreted as evidence of a kinetically trapped, highly unsaturated nucleus that subsequently undergoes slow relaxation toward more filled states, a process that may be hindered in confined pores (Zheng et al., 2026).

By knowing the hydration number and CH_4 concentration in the liquid and hydrate phases, the residual water in fine-grained sediment can be calculated. As noted above, the obtained CH_4 concentration refers to the average concentration of CH_4 in the liquid and hydrate phase. The residual water should be the difference between the amount of water in the whole system and hydrate phase. To clarify the interaction between residual water and hydrate under the hydrate saturation state, the volume ratio of residual water to hydrate (R_{L-H}) is intro-

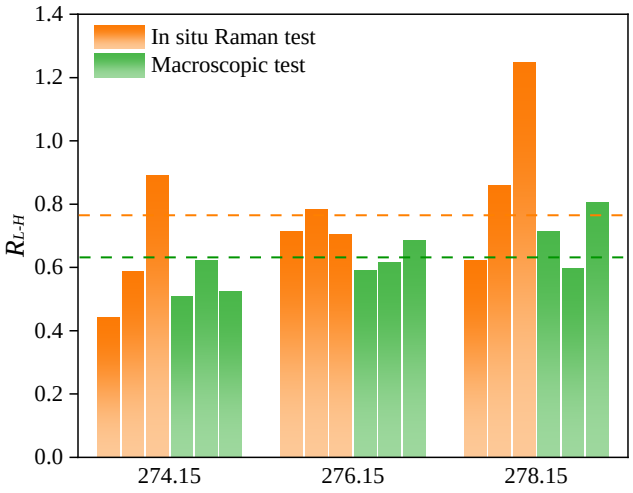


Fig. 6. Volume ratio of residual water to hydrate at a saturated state.

duced, which can be written as (Zhou et al., 2025):

$$R_{L-H} = \frac{V_L}{V_H} = \frac{m_{rw} \cdot \rho_H}{m_H \cdot \rho_w} \tag{1}$$

where V_H and V_L refer to the volume of hydrate and residual water in fine-grained sediment, which can be calculated by knowing the density of hydrate (ρ_H = 0.902 g/cm^3) and liquid water (ρ_w = 1.000 g/cm^3), respectively. The mass of hydrate (m_H) and residual water (m_{rw}) can be written as (Li et al., 2026):

$$m_H = \Delta n_m M_m + \Delta n_m N_H M_w \tag{2}$$

$$m_{rw} = m_w - \Delta n_w N_H M_w \tag{3}$$

where Δn_m represents the amount of CH_4 consumed for hydrate growth, m_w represents the mass of total water molecules including residual water and hydrated water, and M_m and M_w refer to the molecular weight of CH_4 and water, which are 16 and 18 g/mol, respectively. N_H denotes the hydration number, which is 6.54 according to this work. The CH_4 concentrations discussed in Fig. 4 can be expressed as:

$$C_m = \frac{\Delta n_m \cdot M_w}{m_w} \tag{4}$$

By combining Eqs. (1)-(4), R_{L-H} can be further written as follows:

$$R_{L-H} = \frac{(1 - C_m N_H)\rho_H}{\left(C_m \frac{M_m}{M_w} + C_m N_H\right)\rho_w} \tag{5}$$

The density of hydrate was set as 0.902 g/cm^3, which corresponds to fully occupied sI hydrate. Given the low small-cage occupancy, the actual density would be slightly lower (by an estimated $< 5\%$), but this small correction does not affect the main conclusion regarding the residual water fraction. It has been verified that using a reduced density (e.g., 0.88 g/cm^3) changes the calculated R_{L-H} values by less than the experimental uncertainty. The obtained R_{L-H} at saturation state in each *in-situ* Raman measurement are listed in Table 1. Each test is found to have relatively large variation in R_{L-H}, which vary largely from 0.445 to 1.251. Although the R_{L-H} values from individual *in-situ* Raman tests exhibit a relatively wide distribution due to local pore-scale heterogeneity and spectral noise, the averaged values are consistent with the macroscopic measurements, and the overall trend (i.e., residual water fraction of 37%-47%) is reproducible. Generally, 53-63% of pore water converted into hydrate. Although the pressure was kept constantly at 6 MPa, which is highly above the equilibrium pressure, the water in fine-grained sediments did not completely convert into hydrate. The residual water is likely related to the increased capillary pressure caused by the growth of pore-filling hydrates, which may shift the local equilibrium conditions (Yan et al., 2022). Although measurements of capillary pressure were not performed, such an interpretation is one of the potential factors, hence further experiments with varying particle sizes are needed to confirm this hypothesis.

3.2 Hydrate growth in sediment columns

Macroscopic measurements of hydrate growth in sediment columns involve not only the growth of hydrate nuclei in specific sediment pores but also the heat and mass transfer in bulk sediment columns (Zhang et al., 2025). In this case, to minimize the resistance of heat and mass transfer in hydrate formation, the prepared wet sediment sample was compressed into a thin layer and attached to the wall of the reaction vessel.

To enable a robust comparison between microscopic and macroscopic hydrate growth data, the volume ratio of residual water to hydrate (R_{L-H}) is introduced as a common metric. This ratio avoids the need to assume full cage occupancy, which is inappropriate given the highly unsaturated nature of the nuclei observed by *in-situ* Raman. As shown in Fig. 6, the R_{L-H} values derived from the Raman spectra exhibit larger scatter than those from macroscopic measurements, yet their averaged values show good reproducibility, confirming that the overall hydrate inventory is consistently captured by both approaches. In this case, the volume ratio of hydrates to residual water is selected to compare the results from micro- and macroscopic measurements, which can be calculated through Eqs. (1)-(3). The hydration number (N_H) is determined to be 6.54. It is clear that the values of R_{L-H} obtained from *in-situ* Raman show relatively large deviation compared to macroscopic measurements, but the averaged values are not found to differ significantly. Therefore, the hydrate content quantitatively calculated from in-situ Raman spectra is generally consistent with the results obtained from macroscopic measurements.

The relationship between temperature and hydrate growth rate differs greatly from the *in-situ* Raman measurement, as seen in Fig. 7. First, the time for the CH_4 consumption curves to reach stability is significantly longer than that for the CH_4 concentration in hydrates to stabilize in the *in-situ* Raman measurements. Second, the initial gas consumption rate is found to decrease with rising temperature, which is completely opposite to the observations in the in-situ Raman tests.

To explain the inconsistency between macro- and microscopic measurements, it is assumed that CH_4 hydrate growth

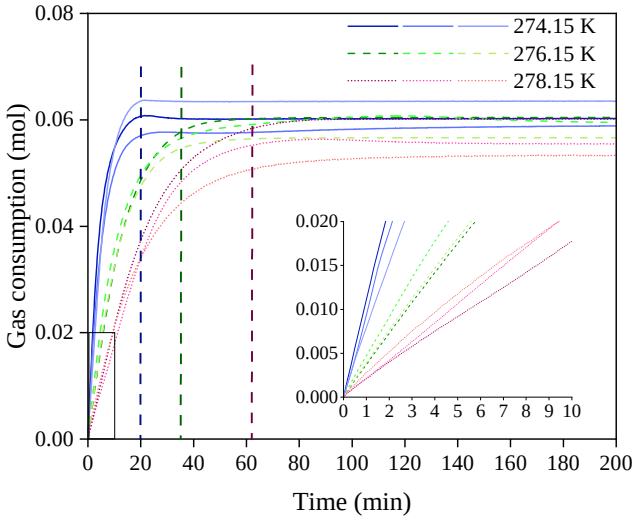


Fig. 7. CH_4 consumptions in hydrate formation in fine-grained sediments.

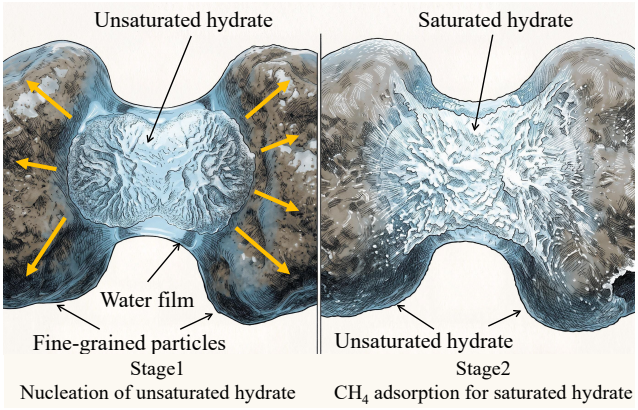


Fig. 8. Schematic diagram of hydrate growth in fine-grained sediments.

in sediments involves more than just one growth mode observed in *in-situ* Raman spectroscopy. The longer time scale required for hydrate formation in macroscopic experiments is mainly due to gas diffusion in the solution phase. Since *in-situ* Raman measurements only focus on the surface of hydrate nuclei, mass transfer resistance including CH_4 dissolution and diffusion in the liquid phase can be ignored. In macroscopic measurements, especially in areas where pore water is relatively concentrated, CH_4 molecules required for hydrate growth must overcome the mass transfer resistance caused by hydrate layer and gas dissolution to reach the hydrate growth front (Zhong et al., 2011; Zhang et al., 2017). Meanwhile, the initial water saturation in the fine-grained sediment in this experiment was only 50%, which resulted in comparatively few areas with relatively concentrated pore water and did not significantly delay the growth of hydrates.

To reconcile the apparent contradiction between the microscopic acceleration of cage filling with temperature and the macroscopic suppression of the initial gas consumption rate, a two-stage growth mechanism is proposed that distinguishes nucleus spreading from gas adsorption. As schematically illustrated in Fig. 8, the growth process consists of the formation and spatial propagation of highly unsaturated hydrate nuclei, followed by CH_4 adsorption onto the existing nuclei. First, under lower temperatures, the spreading of nuclei is promoted, creating abundant adsorption sites, whereas at higher temperatures, although the intrinsic gas adsorption rate is enhanced, the limited nuclei spreading reduces the overall site availability, thereby lowering the net macroscopic consumption rate. Under low temperature conditions, hydrogen bonds in pore water are more likely to form regular hydrate cage structures, allowing highly unsaturated hydrate nuclei to rapidly spread in the pore water, providing more sites for subsequent gas adsorption. However, as the temperature increases, although the gas adsorption rate is improved, the spreading rate of highly unsaturated hydrate nuclei in pore water is inhibited, resulting in a decrease in gas adsorption sites and a reduction in macroscopic gas consumption rate.

4. Conclusions

In this work, CH_4 hydrate growth in fine-grained sediments was investigated through macroscopic and *in-situ* Raman measurements under temperatures ranging from 274.15 to 278.15 K. The obtained Raman spectra were quantitatively analyzed and compared with macroscopic results, resulting in three major findings. First, newly formed hydrate nuclei are highly unsaturated. In the *in-situ* Raman tests, the CH_4 concentration in the large hydrate cage grows rapidly and then approaches a saturation plateau, whereas the CH_4 concentration in the small cage remains low and nearly constant throughout the growth process. Second, pore water in the sediments does not completely convert into hydrate. Under a pressure of 6 MPa, which is well above the equilibrium pressure, approximately 37-47% of the initial pore water remained unconverted in both the macroscopic and the *in-situ* Raman measurements. The presence of pore hydrates was assumed to elevate capillary pressure, thereby suppressing further hydrate growth. Third, the temperature dependence of macroscopic gas consumption rate differed markedly from that of microscopic nucleation. The *in-situ* Raman results showed that increasing the temperature from 274.15 to 278.15 K shortened the hydrate growth time from about 25 to 60 mins and promoted gas adsorption into the large cages. In contrast, macroscopic experiments exhibited a decrease in the initial gas consumption rate with rising temperature, and the time required to reach stability was considerably longer.

On the basis of these findings, a two-stage hydrate growth mechanism was proposed: (1) At lower temperatures, highly unsaturated hydrate nuclei form and spread more rapidly through the pore water, providing abundant sites for subsequent gas adsorption; (2) At higher temperatures, although the intrinsic gas adsorption rate is enhanced, the spreading of nuclei is inhibited, leading to fewer adsorption sites and a reduced net macroscopic consumption rate. Thus, when evaluating the hydrate growth kinetics, it is essential to distinguish nucleation-controlled and mass-transfer-controlled stages.

Acknowledgments

This work was supported by the National Natural Science Foundation of China (No. 42576251).

Conflicts of interest

The authors declare no competing interest.

Open Access This article is distributed under the terms and conditions of the Creative Commons Attribution (CC BY-NC-ND) license, which permits unrestricted use, distribution, and reproduction in any medium, provided the original work is properly cited.

References

Avaji, S., Javanmardi, J., Mohammadi, A. H., et al. The kihara potential function parameters of methane, ethane, propane, and *i*-butane: The effects on clathrate hydrate structure determination. Fluid Phase Equilibria, 2023, 567: 113716.

Chen, G., Liang, D., Kang, Z., et al. Review of hydrogen storage in solid-state materials. Energies, 2025, 18(11): 2930.

Das, S., Tadepalli, K. M., Roy, S., et al. A review of clathrate hydrate nucleation, growth and decomposition studied using molecular dynamics simulation. Journal of Molecular Liquids, 2022, 348: 118025.

Feng, Y., Qu, A., Han, Y., et al. Effect of gas hydrate formation and dissociation on porous media structure with clay particles. Applied Energy, 2023, 349: 121694.

Fukumoto, A., Kamada, K., Sato, T., et al. Numerical simulation of pore-scale formation of methane hydrate in the sand sediment using the phase-field model. Journal of Natural Gas Science and Engineering, 2018, 50: 269-281.

Hu, G., Zhang, Z., Zhao, Y., et al. Formation mechanism and geophysical properties of fracture-filling gas hydrate in the host sediments: A comprehensive review. Earth-Science Reviews, 2024, 258: 104917.

Ke, W., Svartaas, T. M., Chen, D. Y. A review of gas hydrate nucleation theories and growth models. Journal of Natural Gas Science and Engineering, 2019, 61: 169-196.

Kumar, A., Bhattacharjee, G., Kulkarni, B. D., et al. Role of surfactants in promoting gas hydrate formation. Industrial & Engineering Chemistry Research, 2015, 54(49): 12217-12232.

Lee, S., Seo, Y. Experimental measurement and thermodynamic modeling of the mixed CH_4 + C_3H_8 clathrate hydrate equilibria in silica gel pores: Effects of pore size and salinity. Langmuir, 2010, 26(12): 9742-9748.

Li, B., Meng, X., Cheng, T., et al. Affecting mechanism of natural sandstone porous media on the formation and phase equilibrium of methane hydrate. Energy & Fuels, 2024, 38(5): 4091-4101.

Li, M., Zhong, J., Yuan, H., et al. Advances in heat and mass transfer enhancement for gas hydrate formationA review of models, strategies, and conductive materials. International Journal of Heat and Mass Transfer, 2026, 263: 128681.

Liu, H., Wang, S., Fu, Y., et al. The role of clay in hydrate-based carbon emission reduction: Phenomenon, mechanisms, and application. Fuel, 2025, 389: 134575.

Liu, S., A, H., Tang, S., et al. Molecular insights into structural and dynamic properties of water molecules in Calcium silicate hydrate nanopores: The roles of pore size and temperature. Capillarity, 2023, 8(2): 23-33.

Liu, Y., Qi, H., Liang, H., et al. Influence mechanism of interfacial organic matter and salt system on carbon dioxide hydrate nucleation in porous media. Energy, 2024, 290: 130179.

Moridis, G. J., Queiruga, A. F., Reagan, M. T. Simulation of gas production from multilayered hydrate-bearing media with fully coupled flow, thermal, Chemical and geomechanical processes using TOUGH plus millstone. Part 1: Numerical modeling of hydrates. Transport in Porous Media, 2019, 128(2): 405-430.

Mu, L., Cui, Q. Experimental study on the dissociation equilibrium of (CH_4+CO_2) hydrates in the (quartz sands plus NaCl Solution) system. Journal of Chemical and Engineering Data, 2019, 64(12): 6041-6048.

Nikitin, V. V., Dugarov, G. A., Duchkov, A. A., et al. Dynamic in-situ imaging of methane hydrate formation and self-preservation in porous media. Marine and Petroleum Geology, 2020, 115: 104234.

Pang, X., Jia, C., Xu, Z., et al. Application of the whole petroleum system in the evaluation of the global natural gas hydrate resource. Petroleum Exploration and Development, 2025, 52(2): 301-315.

Plee, V., Jaubert, J. N., Privat, R., et al. Extension of the PPR78 equation of state to predict fluid phase equilibria of natural gases containing carbon monoxide, helium-4 and argon. Journal of Petroleum Science and Engineering, 2015, 133: 744-770.

Qin, Y., Shang, L. Y., Lv, Z. B., et al. Methane hydrate formation in porous media: Overview and perspectives. Journal of Energy Chemistry, 2022, 74: 454-480.

Qiu, X., Ji, K., Meng, Q., et al. Evolution chracteristics of methane concentration and microscopic formation mechanisms of methane hydrate: insights from in-situ Raman spectroscopy. Gas Science and Engineering, 2026, 146: 205818.

Rehman, A. N., Bavoh, C. B., Khan, M. Y., et al. Unveiling the potential of CO_2 hydrates in porous media: A review on kinetic modelling, molecular dynamics simulations, and machine learning. Fuel, 2025, 381: 133650.

Rossi, A., Ciulla, M., Canale, V., et al. Constant pressure CO2 replacement of CH4 in different hydrate environments: Structure and morphology. Energy & Fuels, 2023, 37(23): 18968-18976.

Shaibu, R., Sambo, C., Guo, B., et al. An assessment of methane gas production from natural gas hydrates: Challenges, technology and market outlook. Advances in Geo-Energy Research, 2021, 5(3): 318-332.

Sun, C., Liu, S., Li, S., Wang, K., et al. Methane hydrate formation characteristics under different initial conditions and their impact on coal seam properties. Advances in Geo-Energy Research, 2025, 16(3): 229-243.

Sun, Y., Jiang, S., Li, S., et al. Hydrate formation from clay bound water for CO_2 storage. Chemical Engineering Journal, 2021, 406: 126872.

Tegze, G., Pusztai, T., Tóth, G., et al. Multiscale approach to CO_2 hydrate formation in aqueous solution: Phase field theory and molecular dynamics.: Nucleation and growth. Journal of Chemical Physics, 2006, 124(23): 234710.

Uchida, T., Ebinuma, T., Takeya, S., et al. Effects of pore sizes on dissociation temperatures and pressures of methane, carbon dioxide, and propane hydrates in porous media. Journal of Physical Chemistry B, 2002, 106(4): 820-826.

Vitu, S., Privat, R., Jaubert, J. N., et al. Predicting the phase equilibria of CO_2 + hydrocarbon systems with the PPR78 model (PR EOS and kij calculated through a group contribution method). Journal of Supercritical Fluids, 2008, 45(1): 1-26.

Walsh, M. R., Koh, C. A., Sloan, E. D., et al. Microsecond simulations of spontaneous methane hydrate nucleation and growth. Science, 2009, 326(5956): 1095-1098.

Wu, Q., Tang, T., Zhao, Z., et al. Influence of micro-particles on gas hydrate formation kinetics: Potential application to methane storage and transportation. Advances in Geo-Energy Research, 2023, 10(3): 189-199.

Xie, Y., Cheng, L., Feng, J., et al. Kinetics behaviors of CH_4 hydrate formation in porous sediments: Non-unidirectional influence of sediment particle size on hydrate formation. Energy, 2024, 289: 130021.

Yang, D., Yan, R., Cheng, F., et al. Influencing factors of hydration number of synthesized methane hydrates in sediment. Energy & Fuels, 2023, 37(3): 1929-1939.

Yan, R., Lu, D., Song, Y., et al. Modeling the mechanical behavior of methane hydrate-bearing soil considering the influence of temperature and pore pressure. Energy & Fuels, 2022, 36(20): 12510-12523.

Zhang, Y., Li, X., Chen, Z., et al. Formation behavior and controlling factor of methane hydrate in porous media. Proceedings of the 9th International Conference on Applied Energy, 2017, 142: 4044-4049.

Zhang, Y., Liu, L., Luo, L., et al. Permeability prediction in hydrate-bearing sediments via pore network modeling. Advances in Geo-Energy Research, 2025, 16(2): 158-170.

Zhang, Z., Walsh, M., Guo, G. Microcanonical molecular simulations of methane hydrate nucleation and growth: Evidence that direct nucleation to sI hydrate is among the multiple nucleation pathways. Physical Chemistry Chemical Physics, 2015, 17(14): 8870-8876.

Zhao, L., Wang, X., Wu, Y., et al. CO_2 hydrate growth behavior and gas storage capacity in water-absorbing porous media. Chemical Engineering Journal, 2025a, 524: 169069.

Zhao, Y., He, M., Du, Y., et al. Recent advances in molecular mechanisms of gas hydrate growth. Crystengcomm, 2025b, 27(4): 456-467.

Zheng, J., Cheng, F., Li, Y., et al. Progress and trends in hydrate based desalination (HBD) technology: A review. Chinese Journal of Chemical Engineering, 2019, 27(9): 2037-2043.

Zheng, R., Li, X., Negahban, S. Molecular-level insights into the structure stability of CH_4-C_2H_6 hydrates. Chemical Engineering Science, 2022, 247: 117039.

Zheng, X., Duan, J., Yu, W., et al. Investigation into the influence of pore size on methane hydrate decomposition and reformation in confined space. Chemical Engineering Science, 2026, 329: 123840.

Zhong, D., Yang, C., Liu, D., et al. Experimental investigation of methane hydrate formation on suspended water droplets. Journal of Crystal Growth, 2011, 327(1): 237-244.

Zhong, J., Lv, X., Guo, M., et al. Molecular dynamics simulation study on the gas hydrate formation in pores of sediment. Marine and Petroleum Geology, 2025, 174: 107299.

Zhou, X., Zang, X., Long, Z., et al. Multiscale analysis of the hydrate based carbon capture from gas mixtures containing carbon dioxide. Scientific Reports, 2021, 11(1): 9197.

Zhou, X., Xu, C., Wen, H., et al. Thermal stabilities of CH_4 and CO_2 hydrates in quartz sands and modeling. Fluid Phase Equilibria, 2024, 583: 114120.

Zhou, X., Fan, S., Xu, C., et al. Effect of particle size, water saturation, inorganic salt and methane on the phase equilibrium of CO_2 hydrates in sediments. Fluid Phase Equilibria, 2025, 588: 114234.

Zhou, X., Zhou, J., Chen, P., et al. Spectral analysis on the Raman peaks of CH_4, CO_2, and N_2 in the hydrate phase. Energy & Fuels, 2025, 39(3): 1579-1587.

Zhu, L., Wu, S., Zhou, X., et al. Saturation evaluation for fine-gained sediments. Geoscience Frontiers, 2023, 14(4): 101540.

Zuniga, A. R., Li, M., Aman, Z. M., et al. NMR-compatible sample cell for gas hydrate studies in porous media. Energy & Fuels, 2020, 34(10): 12388-12398.